Liquid Crystals
Publication details, including instructions for authors and subscription information:
http://www.informaworld.com/smpp/title~content=t713926090

Phase modulation and ellipticity of the light transmitted through a smectic C* layer with short helix pitch

Evgeny Pozhidaev[a]; Sofia Torgova[a]; Maxim Minchenko[a]; Cesar Augusto Refosco Yednak[bc]; Alfredo Strigazzi[c]; Elio Miraldi[c]
[a] P.N. Lebedev Physical Institute, Russian Academy of Sciences, Moscow, Russia [b] Departamento de Fisica, Universidade Estadual de Maringá, Maringà, Paranà, Brasil [c] Dipartimento di Fisica and CNISM, Politecnico di Torino, Torino, Italy

Online publication date: 16 August 2010

To cite this Article Pozhidaev, Evgeny , Torgova, Sofia , Minchenko, Maxim , Augusto Refosco Yednak, Cesar , Strigazzi, Alfredo and Miraldi, Elio(2010) 'Phase modulation and ellipticity of the light transmitted through a smectic C* layer with short helix pitch', Liquid Crystals, 37: 8, 1067 — 1081
To link to this Article: DOI: 10.1080/02678292.2010.486482
URL: http://dx.doi.org/10.1080/02678292.2010.486482

Liquid Crystals,
Vol. 37, No. 8, August 2010, 1067–1081

Taylor & Francis
Taylor & Francis Group

Phase modulation and ellipticity of the light transmitted through a smectic C* layer with short helix pitch

Evgeny Pozhidaev[a], Sofia Torgova[a], Maxim Minchenko[a], Cesar Augusto Refosco Yednak[b,c], Alfredo Strigazzi*[c] and Elio Miraldi[c]

[a]*P.N. Lebedev Physical Institute, Russian Academy of Sciences, Moscow, Russia;* [b]*Departamento de Fisica, Universidade Estadual de Maringá, Maringà, Paranà, Brasil;* [c]*Dipartimento di Fisica and CNISM, Politecnico di Torino, Torino, Italy*

(*Received 1 March 2010; final version received 13 April 2010*)

A chiral ferroelectric smectic C* liquid crystal (FLC) with the helix pitch $p_0 = 330$ nm was developed to avoid any scattering of visible light when the helix is not unwound over a certain limit. Planar cells with different FLC layer thickness (16 and 44 μm) have been assembled with helix axis parallel to the glass plates and aligned along the rubbing direction. The ellipticity of the light passing through the cells *vs.* the electric field was investigated, and a method for evaluating the electrically controlled birefringence via ellipticity measurements has been established. We have found that the FLC cell is an optical retardation layer driven by the electric field, the effective birefringence being proportional to the square electric field. The physical origin of the electrically controlled phase shift of the light passing through the FLC layer has been analysed.

Keywords: chiral dopant; ferroelectric liquid crystal; helix pitch; ellipticity; phase shift

1. Introduction

It is well known that the most efficient method to obtain a ferroelectric liquid crystal (FLC) multicomponent mixture suitable for electro-optical application is to add a chiral dopant to an achiral smectic C matrix [1, 2]. The dopant belongs to derivatives of p-terphenyl-dicarboxylic acid, which even though non-mesogenic, can increase the temperature range of the C-phase of the mixtures formed with the achiral smectic C matrix [3–5]. We synthesised a new dopant of this series, possessing the highest helical twisting power: the helix pitch in smectic C* mixtures is very short, i.e. $p_o = 200$–350 nm, dependent on the concentration of the dopant [6].

It has already been demonstrated that a short helix pitch FLC ($p_o = 0.4$–0.8 μm) provides an effective phase shift change of a transmitted polarised light beam as a function of the applied electric field intensity [7], but the process has a light scattering by-product because the helix pitch is in the visible range [8]. The new mixtures allow us to overcome this drawback, the helix pitch being in the ultraviolet region. In fact, we obtained a pure electrically controlled phase shift plate based on the electro-optical mode, called deformed helix ferroelectric (DHF) [7]. DHF is a convenient operation mode, able to ensure both low voltage and fast-switching liquid crystalline light shutters, since the response time is less than 200 μs when driving an electric field of around 1 V μm^{-1} [6, 7, 9]. For these reasons we decided to investigate the behaviour of the electrically controlled birefringence in DHF cells when the light scattering and selective light refraction in the visible spectral range are totally suppressed.

When assembling the DHF cell, we treated cell glass plates in order to obtain a planar alignment of the helix axis. This means that in the absence of an external electric field the director alignment in the cell bulk in the C* phase exhibits the expected helix structure, whereas close to the surface a periodic distortion is present, imposing a planar unidirectional orientation; such a deformation becomes less important with greater cell thickness. To this purpose, cells with thicknesses of 16 μm and 44 μm were prepared.

The ellipticity measurement of the light passing through DHF cells is a very precise method of evaluating the cell's optical quality; nevertheless, it has never been done previously, due to the presence of scattering and selective refraction of visible light. We aimed to establish a new method to characterise the optical quality of light scattering and selective refraction-free DHF cells, and to precisely evaluate the electrically controlled birefringence via the ellipticity measurements.

We studied the birefringence modulation of a FLC layer driven by an applied voltage presenting in time the shape of a ($\pm$) step at the frequency of 1 kHz because this frequency is very convenient for measuring. The presence of an external electric field causes anharmonic distortion [10] of the helix structure in the bulk, determining a deviation of the principle optical axes [11], and deeply affecting the polarisation state of the light normally transmitted by the cell. In particular, we measured the intensity of the polarised light transmitted *vs.* the

*Corresponding author. Email: alfredo.strigazzi@polito.it

ISSN 0267-8292 print/ISSN 1366-5855 online

DOI: 10.1080/02678292.2010.486482
http://www.informaworld.com

amplitude of the applied electric field for different values of the angle α formed by the main optical axis of the cell with the polariser, at various orientations of the analyser (from -180° to +180° with respect to the polariser).

The main goal of the present work is to investigate the electrically controlled phase shift $\Delta\Phi$ *vs*. the applied voltage V, according to the following steps:

1. detecting the rotation of the anharmonic helix axis *vs*. the applied voltage intensity;
2. checking whether the cell biaxiality is negligible;
3. measuring the beam ellipticity *vs*. the applied voltage at different values of α, in order to:
   a. characterise the optical quality of the cell;
   b. recognise the dependency of the phase shift and of the effective electrically controlled birefringence Δn_{eff} on the applied electric field intensity E;
   c. evaluate the effective birefringence at $E = 0$.

2. Materials and methods

2.1 Preparation of FLC sample and cells

Qualitative planar alignment, which can provide a contrast ratio approximately equal to 300:1 using white light, was achieved with the use of 4,4'-oxydianiline dianhydride **(PMDA-ODA)** as an aligning layer. The chemical formula of this polyimide after imidisation is reported in Scheme 1.

The application of the aligning film on the ITO surface was done by spin-coating of the PMDA-ODA solution in dimethyl-formamide. The concentration of PMDA-ODA in solution was 0.2–1.5% (weight). The polyimide film was dried on the ITO substrate for 30–40 min at 180°, and imidisation was done at the temperature 275–290° for one hour. The cells were prepared with glassy substrates covered by ITO and aligning films with thickness 20 nm, and the gap was fixed by spacers to 16 μm and 44 μm.

FLC-579, developed at the P.N. Lebedev Physical Institute of Russian Academy of Sciences, was used in the experiments. The helix pitch of this liquid crystal is $p_o = 330$ nm at 23°C, and the refraction indices are $n_{\parallel} = 1.70$, $n_{\perp} = 1.50$; the phase transition sequence is:

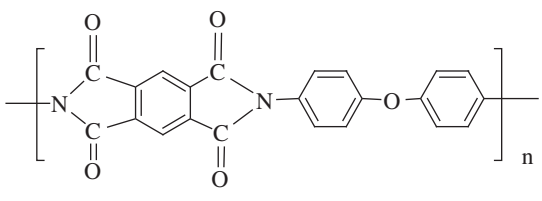

Scheme 1. The chemical formula of 4,4'-oxydianiline dianhydride **(PMDA-ODA)** after imidisation.

$$\text{Cr} \rightarrow 4^{\circ}\text{C} \rightarrow \text{C}^{*} \rightarrow 62^{\circ}\text{C} \rightarrow \text{A}^{*} \rightarrow 109^{\circ}\text{C} \rightarrow \text{Is}.$$

The FLC was inserted into the cell by capillary method in the isotropic phase.

The task is to reach a regular helix alignment in the cell, with the helix axis parallel to the glass plates; the orientation has to be uniform inside each plane parallel to them, and the director gradient has to be practically independent of the distance from the glass plates in the bulk, exhibiting a non-helical flat orientation only close to the surfaces. To this end, it is necessary to apply an alternate electrical training to the FLC layer with a step function of maximum field amplitude in the range 5–9 V μm^{-1} and frequency in the range 0.5 Hz–2 kHz [12]. Acquisition of the correct cell texture has to be confirmed by polarising microscopy. As an example, the results obtained by optical observations are presented in Figure 1 (crossed polarisers). The cell with 44 μm gap considered here had a rather imperfect texture just after filling by FLC-579 (Figure 1(a)), but with a proper electrical training field with a step amplitude of 250 V and frequency from 0.5 Hz–2 kHz, providing a corresponding alternate twisting stress, a better regularity has been reached (Figure 1(b)). By increasing the maximum voltage to 450 V it was possible to obtain a very well-oriented FLC layer (Figure 1(c)).

2.2 Detection of light transmission intensity

Detection of light transmission intensity is the most suitable method for ascertaining information on cell birefringence (either uniaxial or biaxial) and for obtaining the light beam ellipticity and the contrast *vs*. the cell orientation at different values of the applied voltage. We used a linearly polarised light beam (generated either by a He–Ne laser or by a Ga–Ar semiconductor diode laser) normally impinging into the cell. Let us define α_o the angle of the undisturbed helix axis x_o with respect to the polarisation plane, as defined by the polariser P. It can be pre-selected, as can the angle φ of the analyser A with respect to the polariser. A photodiode detects the light transmitted by the system.

It is known [13] that if biaxiality is negligible then Malus' law is valid: we will see that this turns out to be the case in our investigation. Thus, if the cell behaves as an uniaxial optical plate, then ellipticity can be defined as

$$e \equiv \sqrt{\frac{I_{\min}}{I_{\text{MAX}}}}, \tag{1}$$

where $I_{\min}$ and I_{MAX} are the minimum and maximum intensity of the light beam in a definite situation: for

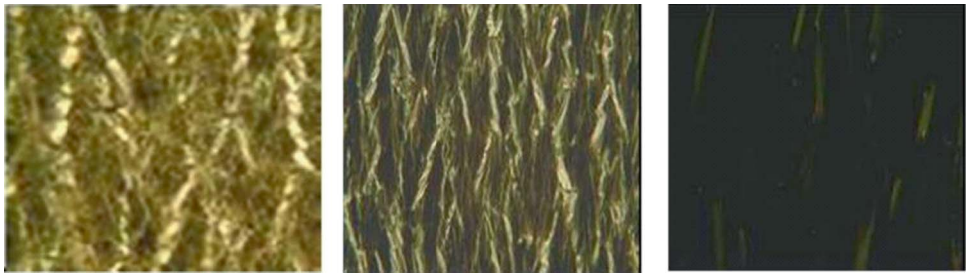

Figure 1. Texture shown by light transmission microscopy images between crossed polarisers through a 44 μm thick FLC-579 layer: (a) without any voltage training after the cell filling; (b) with ± 250 V applied step voltage (frequency from 0.5 Hz to 1.1 kHz); (c) with ± 450 V applied step voltage (same frequency) during 10 min of treatment. The image area is 200 μm × 200 μm (colour version online).

instance, when a constant external voltage is applied to the DHF layer forming a fixed angle α with respect to the polariser P, and the light transmission is considered. From the definition it follows that when a step function is applied the transmitted light beam exhibits two ellipticities $e(+)$, $e(-)$ during the positive and negative peak, respectively. Moreover, if a step function is applied, the *absolute contrast* can be defined as the ratio:

$$c_a \equiv I_{\mathrm{MAX}}/I_{\mathrm{min}} = e^{-2}, \qquad (2)$$

during the application of the same voltage peak, and the *relative contrast* as the ratio between the maximum light intensity during the application of a pulse of one sign, with respect to the actual light intensity for the pulse of opposite sign:

$$c_r \equiv \mathrm{MAX}[I(+), I(-)]/\min[I(+), I(-)]. \qquad (3)$$

In Equation (3) the numerator is the larger intensity between $I(+)$ and $I(-)$, whereas the denominator is the smaller one in the same cell condition. Obviously, for every given configuration α, there are two absolute contrasts, $c_a(+)$, $c_a(-)$, as well as the ellipticities, whereas there is only one relative contrast. For instance, in the ideal case when both ellipticities are zero, the absolute contrasts are infinite. If $I(+) = I(-)$, then the relative contrast $c_r = 1$.

If no voltage is applied to the cell, the helix is harmonic (at least in the bulk), and for $\alpha_o = 0^\circ$ the light transmitted is linearly polarised in the plane $[X, Z]$, along $x_o \parallel X$, if the cell is uniaxial, and the maximum transmission occurs for $\varphi = 0^\circ$ (the same happens for $\alpha_o = 90^\circ$: in this case, the light transmitted is linearly polarised along y_o), see Figure 2. Moreover, the cell being uniaxial, when no external field is applied and $0^\circ < \alpha_o < 90^\circ$, both light field components x_o, y_o are transmitted, and the cell behaves as a $(k\lambda)$-plate, where k is *a priori* a real number. In particular, if $k = n$, where n is a positive integer, then the polarising plane of the light transmitted by the cell is the same of the impinging light beam.

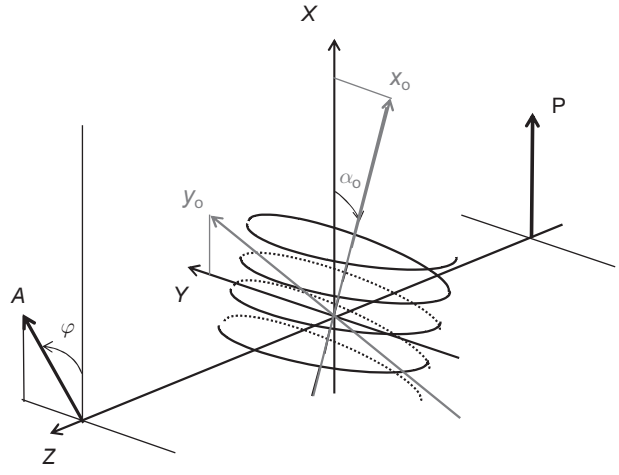

Figure 2. Scheme of FLC cell with glass plates parallel to the vertical plane $[X, Y]$ fixed in the laboratory. The cell is placed between polariser P and analyser A; A is at an angle φ with respect to P. In the absence of any applied electric field, the helix is regularly harmonic in the bulk. Its axis x_o forms an angle α_o with the same direction. The light beam propagates along the Z-direction. The maximum intensity of the transmitted light beam occurs when the cell is rotated to either $\alpha_o = 0^\circ$, or $\alpha_o = 90^\circ$, and $\varphi = 0^\circ$.

If $k = (2n - 1)/4$, the transmitted light beam is elliptically polarised, counter clockwise when n is odd, or clockwise when n is even, respectively: hence, in the special case when $\alpha_o = 45^\circ$, it is circularly polarised. If $k = 1/2$, the transmitted light is linearly polarised, with the polarisation plane rotated by an angle $\psi = (180^\circ - 2\alpha_o)$ with respect to the incident one (for $\alpha_o = 45^\circ$, we have $\psi = 90^\circ$) [14]. When a voltage step function [(+)(−)] at certain frequency is applied to the cell, the electric field linearly couples with the FLC polarisation vector, inducing a distortion in the helix alignment, which becomes anharmonic [10]. As a result, the helix molecular director undergoes a periodic deformation,

which is locally stronger the closer to 180° the initial orientation angle of the permanent polarisation with respect to the applied electric field becomes. The distortion turns out to be dependent on the sign of the applied electric field. Consequently, the anharmonic helix axis appears to rotate one way during the application of a positive voltage constant peak (Figure 3), and in the opposite way when a negative constant peak is applied: moreover, the rotation angle $\Delta\alpha$ depends on the field intensity [11].

The distance between smectic planes where no deformation occurs remain unchanged, corresponding

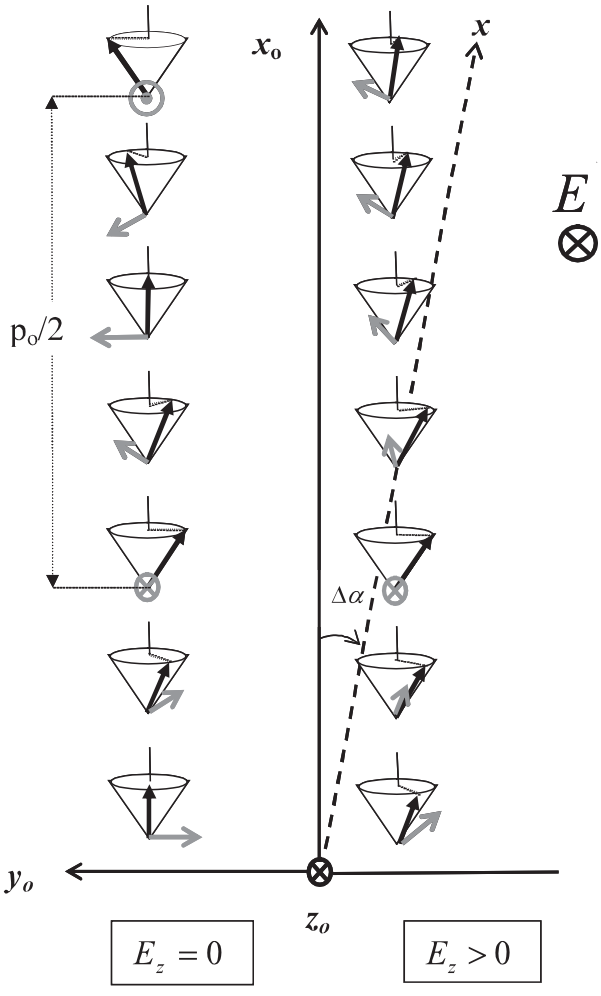

Figure 3. The origin of the DHF effect is presented. The $[x_o,y_o]$-plane parallel to the cell plates is shown. The black arrows represent the smectic C* director $\bar{n}$, the dotted lines the in-plane director $\bar{c}$, and the grey arrows the local spontaneous polarisation $\vec{P}$ of smectic layer. In the absence of an external field (on the left side, $y_o > 0$) the helical order is harmonic, with pitch p_o and helix axis x_o. On the right side ($y_o < 0$) the applied electric field $\vec{E}$ obliges $\vec{P}$ to turn as much as the distance from the starting alignment. It is evident that a periodic anharmonicity is induced and that the helix axis is tilted towards the x-axis (which still belongs to $[x_o,y_o]$-plane).

to the initial helix pitch p_o, but the actual pitch of the anharmonic helix becomes $p = p_o/\sin\Delta\alpha$, increasing with the applied field E. In the ideal case, if $E\rightarrow\infty$, then $\Delta\alpha\rightarrow\theta$ and the helix disappears, becoming completely unwound: the smectic C* has the same alignment as the so-called Surface Stabilised FLC structure (SSFLC) [15]. This means that when an external step function is applied to the cell, its birefringence turns out to be modulated by the external field itself, if the frequency is less than 100–150 kHz [16]: the cell then behaves as an electrically controlled uniaxial birefringent plate. The same situation already discussed in the absence of voltage is valid, provided α_o is replaced in the presence of the voltage by ($\alpha_+ = \alpha_o + \Delta\alpha_+$) and by ($\alpha_- = \alpha_o + \Delta\alpha_-$), when positive and negative voltage peaks are applied.

We will evaluate α_+, α_- *vs.* the applied voltage V, taking into account that in this condition, with the actual helix axis parallel (or perpendicular) to the polariser P, the light transmission intensity presents a maximum when $\varphi = 0°$ and a minimum when $\varphi = 90°$. The results are expected to be the same when no field is applied for $\alpha_o = 0$ (undistorted helix axis parallel to P) and for $\alpha_o = 90°$ (undistorted helix axis perpendicular to P). The optical behaviour of the DHF cell allows us to calculate the contrast and the ellipticity of the polarised light beam transmitted through the cell for particular values of the actual helix axis alignment α; of particular interest are the values $\alpha_{1+} = \alpha_+$, $\alpha_{2+} = \alpha_+ \pm 45°$, and $\alpha_{3+} = \alpha_+ \pm 90°$ when the positive voltage peak is considered (in the case of negative peaks the symmetric values $\alpha_{1-} = \alpha_-$, $\alpha_{2-} = \alpha_- \pm 45°$, $\alpha_{3-} = \alpha_- \pm 90°$ have to be taken into account).

In fact, discussing only the positive peak for simplicity, the cell always behaves as a ($k\lambda$)-plate, where k is *a priori* a real number, as well as when no field is applied.

1. $k = n$. If $k = n$ (with n an integer), then the polarising plane of the light transmitted by the cell is the same as the impinging light beam. Hence, independently of $\alpha = \alpha_{1+}, \alpha_{2+}, \alpha_{3+}$ we have in the ideal situation $I_{MAX}(\varphi = 0°) = I_o$, $I_{min}(\varphi = 90°) = 0$; with ellipticity $e \equiv \sqrt{\frac{I_{min}}{I_{MAX}}} = 0$, $I(\varphi = 45°) = I(\varphi = 135°) = I_o/2$, with always $e = 0$, since e of the transmitted light depends only on α.
2. $k = (2n-1)/4$. If $k = (2n-1)/4$, the cell behaves as a $\lambda/4$ or $3\lambda/4$ plate; then the transmitted light beam is, in principle, elliptically polarised, counterclockwise or clockwise, respectively: in particular, when $\alpha = \alpha_{1+}$, the optical ellipse degenerates to a linear polarisation along the actual helix axis x, and the resulting pattern is the same as before. When $\alpha = \alpha_{2+}$, the transmitted light is circularly

polarised, then: $I(\varphi = 0^\circ) = I_o/2$, $I(\varphi = 90^\circ) = I_o/2$, with ellipticity $e = 1$, as for $\varphi = 45^\circ$, $\varphi = 135^\circ$ as well. When $\alpha = \alpha_{3+}$, the situation is symmetrical with respect to the first one, with the optical ellipse degenerated along the normal y to the actual helix axis.

3. $k = n - 1/2$. If $k = n - 1/2$, the cell behaves as a $\lambda/2$ or $3\lambda/2$ plate; then the transmitted light is linearly polarised, with the polarisation plane rotated by an angle $\psi = (180^\circ - 2\alpha)$ with respect to the incident one. Hence, when $\alpha = \alpha_{1+}$, we have $\psi = 180^\circ$ along the actual helix axis x, and the resulting pattern is the same as in case 1. When $\alpha = \alpha_{2+}$, then $\psi = 90^\circ$: the emerging light beam is linearly polarised along the normal y to the actual helix axis. This means that $I_{MAX}(\varphi = 90^\circ) = I_o$, $I_{min}(\varphi = 0^\circ) = 0$; with reverse ellipticity $e \equiv \sqrt{\frac{I_{min}}{I_{MAX}}} = 0$, $I(\varphi = 45^\circ) = I(\varphi = 135^\circ) = I_o/2$, and ellipticity remains the same, $e = 0$. When $\alpha = \alpha_{3+}$, we have $\psi = 0^\circ$, which is again indistinguishable from the situation $\psi = 180^\circ$.

In Figure 4, the polarisation of the transmitted light beam for certain angles of the cell with respect to the polariser is shown schematically.

When discussing cell behaviour as an optical layer, it should be noted that this is the same as referring to a $k\lambda$-plate or to a $2k\pi$-plate, but quoting the phase retardation instead of the path difference between extraordinary and ordinary beam.

2.3 *Ellipticity and contrast at peculiar orientations of helix axis*

In Table 1 the ideal pattern of ellipticity e for different behaviours of the cell as an optical plate is mapped. We note that, since the transmitted light electric field square amplitude is $E_L^2 = E_{Lx}^2 + E_{Ly}^2$, when the transmitted light beam is circularly polarised the impinging intensity $I_o = 2I$, where I is the intensity of the transmitted light beam, which always affects the analyser regardless of direction. From Table 1 it is evident that to understand whether the cell driven by a certain

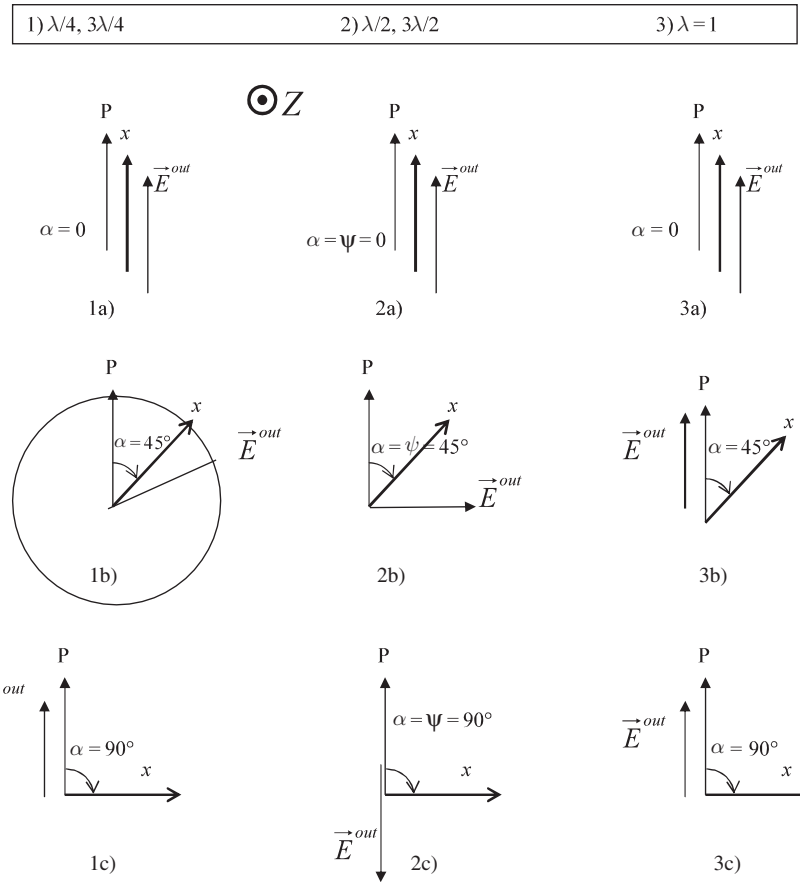

Figure 4. Drawing of scheme of the electric field of the transmitted polarised light beam for particular angles of the actual helix axis x with respect to the polariser P in the ideal case. The light beam propagates along the z-axis (towards the reader). Interesting information is found when the analyser A is parallel or perpendicular to P ($\varphi = 0^\circ$, 90°, respectively), or forms with P an angle $\varphi = -45^\circ$, 45°.

Table 1. Scheme of transmitted light intensity and of ellipticity for particular helix axis orientations in the ideal case (the grey part of the Table illustrates the 45° inclination of the helix axis x with respect to P).

		$\lambda/4$		$\lambda/2$		λ	
α	φ	I vs I_o	e	I vs I_o	e	I vs I_o	e
$\alpha_1 = 0\ \alpha_3 = 90°$	$\varphi = 0°$	$I_{MAX} = I_o$	0	$I_{MAX} = I_o$	0	$I_{MAX} = I_o$	0
	$\varphi = 90°$	$I_{min} = 0$		$I_{min} = 0$		$I_{min} = 0$	
	$\varphi = 45°$	$I = I_o/2$	0	$I = I_o/2$	0	$I = I_o/2$	0
	$\varphi = 135°$	$I = I_o/2$		$I = I_o/2$		$I = I_o/2$	
$\alpha_2 = 45°$	$\varphi = 0°$	$I = I_o/2$	1	$I_{min} = 0$	0	$I_{MAX} = I_o$	0
	$\varphi = 90°$	$I = I_o/2$		$I_{MAX} = Io$		$I_{min} = 0$	
	$\varphi = 45°$	$I = I_o/2$	1	$I = I_o/2$	0	$I = I_o/2$	0
	$\varphi = 135°$	$I = I_o/2$		$I = I_o/2$		$I = I_o/2$	

electric field acts as a $\lambda/4$–, or $\lambda/2$–, or λ-layer, it is necessary to examine the light transmitted at the cell orientation $\alpha \equiv \alpha_2 = 45°$, since in this case it is possible to discriminate between linear polarisation along the x-axis, y-axis, 45°-axis, and circular polarisation. Moreover, this orientation provides the best condition for obtaining interference between ordinary and extraordinary beams, allowing us to maximise the information concerning birefringence of the spatially non-uniform optical plate. Eventually, only $\alpha \equiv \alpha_2 = 45°$ allows us to specify the cell birefringence type. In contrast, either $\alpha \equiv \alpha_1 = 0°$ or $\alpha \equiv \alpha_3 = 90°$ are essential for measuring the uniformity of the sample alignment, i.e. the optical quality of the cell.

3. Experiment and results

3.1 Set-up

The set-up scheme of the polarised light transmission experiment is shown in Figure 5. The optics system lies on an optical table, which is mechanically isolated from the electronic system support in order to avoid vibrations.

The polarising plane of the polariser P is fixed during the experiment, whereas the orientation angle α with respect to P of the actual helix axis of the DHF cell can be pre-selected, along with the angle φ of the analyser A with respect to P. Oscilloscope 1 allows us to record both the voltage step function applied to the cell and the transmitted light intensity (in arbitrary units). The data are recorded by a computer.

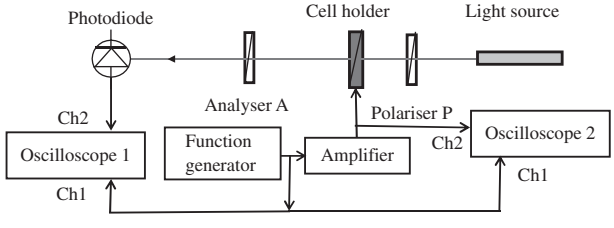

Figure 5. Drawing of the experimental set-up for polarised light transmission measurements. The light source used was either a He–Ne laser (λ= 0.63 μm) or a Ga–Ar semiconductor diode laser (λ= 0.65 μm).

3.2 Anharmonic helix axis

Typical data are presented in Figure 6, which shows that on applying a (40 V_{pp}, 1– kHz)-step voltage, the maximum intensity of the transmitted light beam when the positive pulse is applied no longer occurs for $\alpha = 0°$, or 90°, but for $\alpha_+ = -17°$, or 73° (in particular, the latter is seen).

It is evident from Figure 6 that the conditions of maximum intensity transmission occur at a different rotation angle α_- when the applied pulse is negative: $\alpha_- - \alpha_{o-}$ is expected to be symmetric with respect to α_+-α_o. The measurements performed on the 16 μm DHF

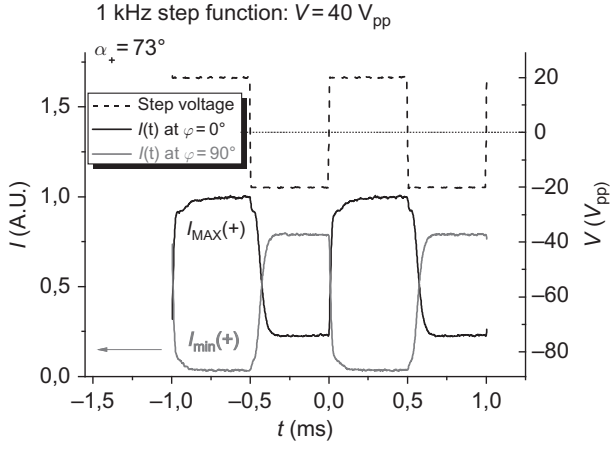

Figure 6. Typical behaviour in time of the polarised light beam intensity transmitted through a 16 μm DHF cell (in arbitrary units) *vs.* an applied (40 V_{pp}, 1 kHz)-step function. This cell orientation ($\alpha_+ = 73°$) corresponds to a maximum transmission when the positive voltage is applied, the actual helix axis is normal to the polariser P and $\varphi = 0°$ (analyser A parallel to P). The anharmonic helix axis is rotated by the angle $\alpha_+ - \alpha_o = -17°$ with respect to the undisturbed one.

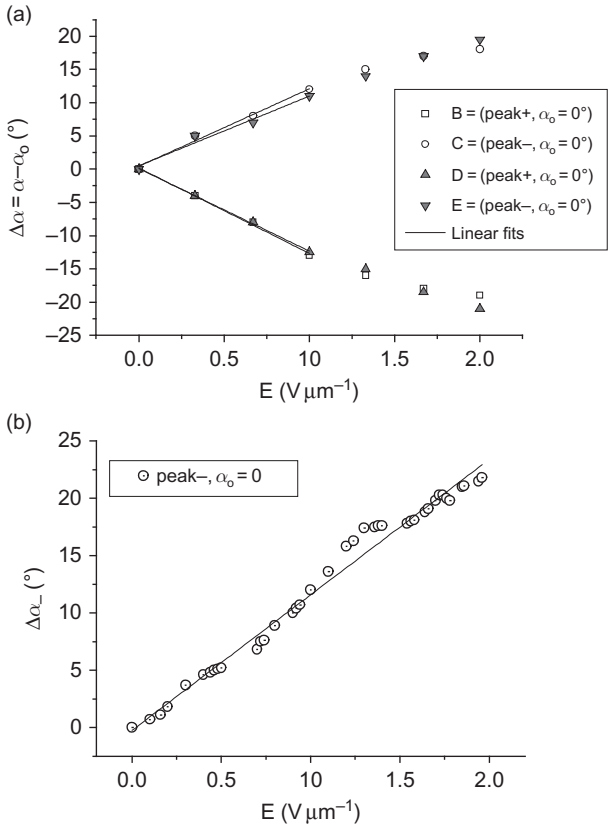

Figure 7. Rotation angle ($\alpha - \alpha_o$) of the actual helix axis *vs.* the external voltage applied to a DHF cell measured looking for the maximum light transmission with analyser A parallel to polariser P (i.e. with $\varphi = 0$): a) 16 μm cell. Note that the data relevant to the actual helix axis parallel to P and normal to it are the same, as expected; b) 44 μm cell. In both cases the data describe for small amplitude field a linear behaviour $\Delta\alpha$ *vs. E*. By computing the linear regression only, field values smaller than 1 V μm^{-1} were taken into account.

cell confirm this behaviour. Moreover, the experimental data satisfy a linear trend of $\Delta\alpha$ *vs. E* with a 99% level of confidence, at least in the range 0–40 V_{pp}, corresponding to the field range 0–1.3 V μm^{-1} (Figure 7).

It is possible to show that, if the director polar angle $\theta < 45°$, the applied electric field $E < E_c$, where E_c is the critical field for helix unwinding at zero frequency, and the operating frequency is definitely smaller than a characteristic frequency of FLC material, then the rotation angle $\Delta\alpha$ of the anharmonic helix axis can be considered as proportional to E when $\Delta\alpha < \theta$ (see Appendix, Equations (19A) and (21A)). The angular coefficient of the linear regression $\Delta\alpha$ *vs. E* is given by

$$b = \frac{\frac{\pi^2}{64E_c}\sin 2\theta}{1 - \frac{3}{2}\sin^2\theta}. \tag{4}$$

This allows us to obtain an estimate of the critical field E_c for the helix unwinding at zero frequency; the lack of precision is due to the fact that in the frame of validity of Equation (19A) it is necessary to consider only data which satisfy the condition $E < E_c$, and the material characteristic frequency is considered to be infinite, whereas in the frame of the present measurements it has been estimated at about 5.5 kHz. From Equation (4), the angular coefficient b computed from data of the linear regression $\Delta\alpha$ *vs. E* relevant to both DHF cells presented in Figure 7 provides

$$E_c = \frac{\pi^2 \sin 2\theta}{64\left(1 - \frac{3}{2}\sin^2\theta\right)b}. \tag{5}$$

From the data of Figure 7 comprising only $E < 1$ V μm^{-1}, we obtained in the case of the 16 μm cell: $b = 0.2048$ μm V^{-1}; in the case of the 44 μm cell: $b = 0.1689$ μm V^{-1}.

Since the FLC material is characterised by $\theta = 31°$, the evaluation in the first case turns out to be E_c (16 μm) ≈ 1.1 V μm^{-1}, whereas in the second case E_c (44 μm) ≈ 1.3 V μm^{-1}. We have to underline that this only gives the evaluation of E_c at zero frequency, and only an order of magnitude of E_c at 1 kHz. In fact it is expected to be greater than 1 V μm^{-1}, since E_{MAX} of plots in Figure 7 corresponds to $\Delta\alpha_{MAX} = 20°$, whereas it has to be $\Delta\alpha(E_c) = \theta = 31°$. The expected value of E_c (1 kHz) is about 3 V μm^{-1} [17].

As reported in the Appendix, the angular coefficient b can be expressed in terms of the material parameter $G \equiv \frac{\varepsilon_o \chi_G}{P_S}$, where ε_o is the vacuum permittivity, $P_S = 1.2\times10^{-3}$ C m^{-1} is the spontaneous polarisation, and χ_G is the susceptibility of Goldstone mode, which can be related to the FLC elastic constant K: hence such parameters can be indirectly measured from the experimental data shown in Figure 7. The result of the parameter evaluation is presented in Table 2. Note that G can be considered as a reduced susceptibility.

3.3 Data consistency with Malus' law

In Figure 8 the light transmission data are reported for the same conditions as in Figure 6: a 40 V_{pp} step function is applied to the cell, causing anharmonicity in the helical sample alignment and determining a rotation of

Table 2. Indirect measurement of material parameters from experimental data relevant to anharmonic helix axis rotation. Note that also χ_G is reported in SI.

DHF-cell thickness (μm)	G (μm/V)	E_c (V/μm)	χ_G	K (10^{-11}N)
16	0.2793	1.1	31	2.2
44	0.2304	1.3	38	2.7

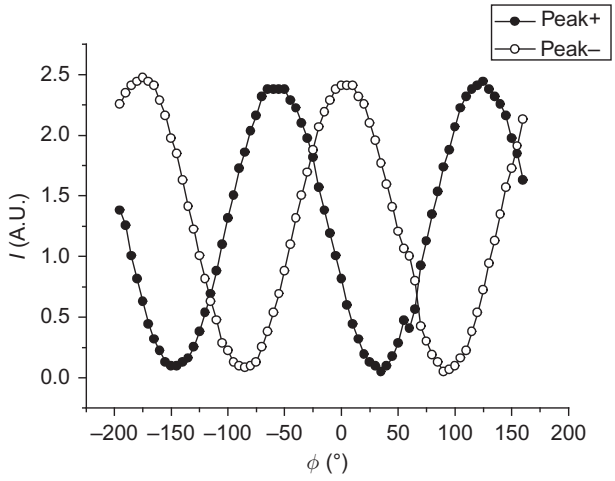

Figure 8. Polarised light intensity I (in arbitrary units) transmitted through the 16 μm thick DHF cell *vs.* the angle φ of the analyser A with respect to the polariser P. The light beam had wavelength $\lambda = 0.65$ μm. The cell was driven by a 40 V_{pp}-step voltage with 1 kHz frequency. Note that 40 V_{pp} corresponds to a field $E = 1.33$ V μm^{-1}. The actual anharmonic helix axis during the application of the positive (negative) peak voltage is rotated with respect to the harmonic helix axis by the angle $\alpha_+ = -17°$ ($\alpha_- = 16°$).

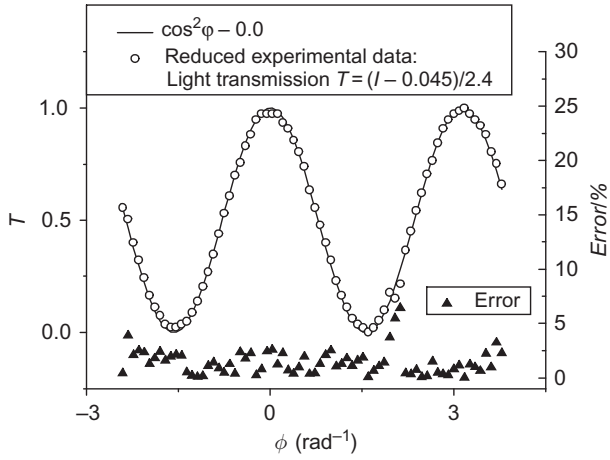

Figure 9. Malus' law is well verified by polarised light transmission, according to experimental data reported in Figure 8. Only the anharmonic helix due to the positive peak voltage is considered here, since the result of the statistical analysis for the symmetric condition is the same. Transmission data are normalised to maximum = 100%, and angle φ between A and P is given in rad.

–17° (+16°) of the helix axis when positive (negative) voltage is applied (the difference between the two absolute experimental values is due to the measurement uncertainty). An arbitrary angle $\alpha = 103°$ between the undisturbed helix axis and polariser P was considered for this analysis, which follows the same procedure, and has the same result, independent of the particular value of angle α. The light transmission is detected *vs.* the angle φ between analyser A and polariser P with interval step $\Delta\varphi = 5°$ in the range (–180°, +180°). Both experimental curves given by the application of positive and negative voltage peaks are given here: the first is shifted left by ~(–35°) with respect to the undisturbed helix transmission curve, and the second is shifted right by the same value ~35°.

The experimental data have been normalised and fitted with $\cos^2\varphi$ curve, in order to find whether Malus' law is satisfied. In Figure 9 the analysis result is reported only for the positive voltage peak. There is good agreement between the data and the model, the average error being kept within 2% (and the maximum error within 5%). The same behaviour was obtained for the similar negative peak voltage curve.

3.4 Ellipticity measurements

Since the DHF cell light transmission behaves according to Malus' law, we can consider it as a uniaxial birefringent plate and use it for experimental evaluation of the ellipticity of Equation (1). We measured the ellipticity at particular orientations of the helix axis *vs.* the applied step voltage in the range 0–60 V_{pp} at 1 kHz, and found that the cell is an electrically controlled birefringence layer. For example, the results from the 16 μm cell are reported in Table 3, when the external voltage is $V = 20$ V_{pp}, applied as a step function, and the distorted helix axis forms an angle of 45° with respect to P in both cases, $V(-) = -10$ V_p(voltage peak -), and $V(+) = 10$ V_p(voltage peak +). The transmission with parallel and crossed (A, P) is about $I_o/2$, half of the maximum light intensity; the ellipticities turn out to be about 0.88, the contrasts about 1.4: at this driving voltage the cell behaves as a ($\lambda/2$) optical layer (Table 1).

In any case, we may note the difference between the ideal and actual cases: in the experiment with the 16 μm cell we never obtained ellipticity $e = 0$, or $e = 1$. Our minimal data are about $e = 0.17$ (when $\alpha = 0°, 90°$, and our maximal data about $e = 0.88$ (when $\alpha = -45°, 45°$).

As noted in Table 1 for the ideal case, the ellipticity at α–α_o =0 gives no information regarding the birefringence, but indicates the FLC layer alignment quality in the same sense as the contrast ratio does, see Equation (2). The best DHF cell alignment quality (Figure 1(c)) was achieved with the 44 μm thick FLC-579 layer. This alignment quality depends on the applied voltage, as illustrated by the ellipticity and the contrast ratio, measured at α–$\alpha_o = 0$ (Figure 10).

Such a perfect DHF cell alignment, providing the contrast ratio c_a = 200:1–300:1 with ellipticity 0.073–0.060, according to (2), has not been obtained for DHF cells by other authors [18, 19], who used FLC layer thickness less than 10 μm, nor by us with the

Table 3. Example of light transmission data of DHF 16 μm cell at $V = 20\ V_{pp}$, 1 kHz for positive and negative values of the step function: intensity, ellipticity, absolute contrast, when the deformed helix axis forms an angle of 45° with respect to the polariser P (columns 2–6). Column 3 shows the analyser orientation (φ =0°, or 90°). In the last part of the Table the same parameters for the other peak of the step function and the relative contrast are reported. Since the maximum intensity crossing the cell is in arbitrary units $I_o = 5.5$, for this voltage the cell behaves almost as a (λ/4)-optical retarder.

V/20Vpp	α(±) – 45°	φ	*I*(±) /A.U.	*e*(±)	c_a(±)	*I* /A.U.	*e*	c_a	c_r
1	α(–) = 7°	0°	2.40625	0.86	1.4	3.34375	0.85	1.4	1.4
		90°	3.25			2.4375			
	α(+) = –8°	0°	2.4375	0.86	1.4	3.1875	0.87	1.3	1.3
		90°	3.3125			2.4375			

16 μm cell, where ellipticity at $\alpha - \alpha_0 = 0$ is 0.17. The improved alignment only occurs with a very thick FLC layer. The probable reason is that in a FLC layer with higher thickness the helix distortion near solid aligning surfaces has lesser importance with respect to the bulk regular orientation.

The dependence on the applied voltage of the ellipticity $e_+(45^o; V)$, due to positive voltage peak for a 44 μm thick DHF cell filled with FLC-579, measured at $\alpha \equiv \alpha_2 = 45^\circ$ is reported in Figure 11; it is similar to the experimental behaviour of the function $e_-(45^o; V)$. Such a dependence allows us to evaluate the electrically controlled birefringence $\Delta n_{eff}(E)$during the same voltage peak.

The background for this evaluation is the relationship between the total birefringence $\Delta n_{\text{eff}}^{\text{TOT}}$ in the presence of applied electric field and the relevant total phase shift $\Delta\Phi^{\text{TOT}}$ between extraordinary and ordinary light beams transmitted by the DHF cell:

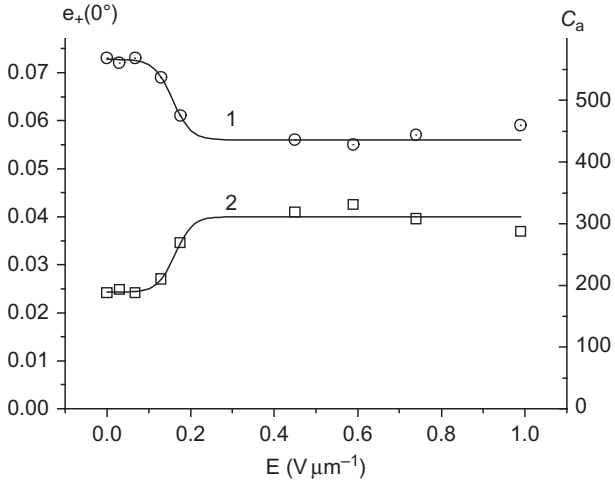

Figure 10. Dependence on the applied electric field E of the ellipticity $e_+(0^\circ)$ (curve 1) and of the contrast ratio c_a (curve 2). The light beam had wavelength $\lambda = 0.65$ μm. It was passing through the 44 μm-thick DHF cell, the texture of which is shown in Figure 1(c). Measurement performed at $\alpha - \alpha_0 = 0$, i.e. with undisturbed helix axis parallel to P.

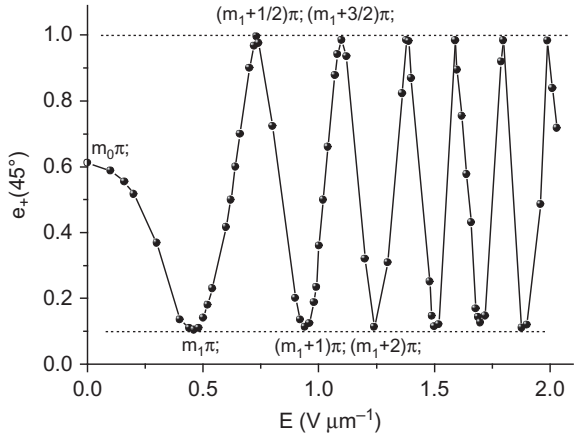

Figure 11. Dependence on applied field of the ellipticity $e_+(45^\circ)$ of 44 μm-thick DHF cell filled with FLC-579, measured at wavelength 0.65 μm.

$$\Delta\Phi^{\text{TOT}} = \frac{2\pi}{\lambda}\Delta n_{eff}^{\text{TOT}} d_{\text{FLC}} = \frac{2\pi}{\lambda}\left[\langle n_e(\theta, \varphi_c(E;x)\rangle - n_o\right] d_{\text{FLC}}, \quad (6)$$

where n_e is the extraordinary index of refraction, $\theta, \varphi_c(x)$ are the smectic director polar angle and azimuth, respectively, n_o is the ordinary index of refraction, and $\langle\ \rangle$ represents the average over one pitch. By putting

$$\begin{cases} \Delta n_{\text{eff}}(E=0) \equiv \langle n_{\text{e}}(\theta, \varphi_{\text{c}}(E=0;x)\rangle - n_o \\ \Delta n_{\text{eff}}(E) \equiv \langle n_{\text{e}}(\theta, \varphi_{\text{c}}(E;x)\rangle - \langle n_{\text{e}}(\theta, \varphi_{\text{c}}(E=0;x)\rangle \end{cases}, \quad (7)$$

the phase shift can be written as

$$\Delta\Phi^{\text{TOT}} = \Delta\Phi_{\text{o}} + \Delta\Phi(E) = \frac{2\pi}{\lambda}\left[\Delta n_{\text{eff}}(E=0) + \Delta n_{\text{eff}}(E)\right] d_{\text{FLC}}, \quad (8)$$

where d_{FLC} is the FLC layer thickness, λ is the wavelength, $\Delta n_{\text{eff}}(E=0)$ is the effective birefringence of

the helical structure in the absence of external electric field, and $\Delta n_{\text{eff}}(E)$ is the effective electrically controlled birefringence due only to the field application. Note that Equation (8) is valid no matter what the magnitude of $\Delta n_{\text{eff}}(E)$ is with respect to the first term $\Delta n_{\text{eff}}(E=0)$. Evidently, in any situation the total phase shift can be expressed as

$$\Delta\Phi^{\text{TOT}} = m\pi, \tag{9}$$

where m is a real number. Note that the initial phase shift $\Delta\Phi_o$ must be considered as an angle mod 2π (i.e. $0 \leq \Delta\Phi_o < 2\pi$), since m_o and $m_o+2n\ \pi$ (n being an integer) are optically indistinguishable.

The particular situation when m is an integer also corresponds to $e_+(45^o) = 0$, whereas all semi-integer values of m correspond to $e_+(45^o) = 1$, as was clarified previously for the ideal case. In particular, let us define m_1 as the integer value of m which corresponds to first minimum of the ellipticity $e_+(45^o, V)$ *vs. V*. Under this definition, the minima of $e_+(45^o, V)$ correspond to phase shifts $m_1\pi$; $(m_1+1)\pi$; $(m_1+2)\pi\ldots$, while maxima to $(m_1+1/2)\pi$; $(m_1+3/2)\pi\ldots$, as shown in Figure 11. In fact, we can see that in reality the minimal magnitude of the ellipticity is $e_+(45^o) \simeq 0.1$ instead of $e_+(45^o) = 0$, as is expected for the ideal case. Nevertheless, we will presume that due to continuity these minima correspond to the phase shifts $m_1\pi$; $(m_1 + 1)\pi\ldots$, the small ellipticity being the consequence of the lack of perfect alignment. Thus, the oscillations of $e_+(45^o)$ as a function of V between the limits $e_+(45^o) = 0.1$ and $e_+(45^o) = 1$ observed in the experiment can be explained by the increasing magnitude of m, due to $\Delta n_{\text{eff}}(E)$ increasing due to helix axis rotation driven by the external field, according to Equations (6) and (7). Note that the phase shift between a minimum and an adjacent maximum of the experimental dependence is exactly $\pi/2$, whereas the shift between two adjacent minima and two adjacent maxima is exactly π.

To distinguish whether in the first (and in the second) minimum the cell behaves as a ($\lambda/2$)- or a λ-type optical layer, it is sufficient to check the analyser orientation providing the maximum transmittance (Figure 4 and Table 2). Since in our experiment the first minimum (at 23 V_{pp}) gives the maximum transmittance for parallel polarisers, this means that the layer behaves in that condition as λ-type, i.e. m_1 is the first even number ($m_1 = 2$), whereas in the second minimum (at 47 V_{pp}) the cell must behave as ($\lambda/2$)-optical layer; this is confirmed by the fact that in this condition the maximum transmittance works with crossed polarisers (Figure 4 and Table 2).

Now the following problem arises: what is the limit m_o of m when V approaches zero? Certainly, it is not an integer, since it has to be $m_1 - 1/2 < m_o < m_1$, meaning $3/2 < m_o < 2$, due to the fact that before the first minimum there is no maximum with ellipticity $e = 1$. As an approximate linear evaluation, we propose the relation

$$m_1 - m_o = (1 - e)/2, \tag{10}$$

providing $m_o = 2 - 0.38/2 = 1.81$. In this manner the initial retardation (mod 2π) has been estimated. Thus we have provided an alternate method of calculating the phase shift $\Delta\Phi_0$ in the absence of an external electric field which does not require transmittance spectral measurements, as has been done previously [17].

The above explanation is sufficient to evaluate the total phase shift as defined in Equation (9), where $m = m_1$; $m_2 = m_1+1/2$; $m_3 = m_1+1$, etc. correspond to alternate minima and maxima of the ellipticity *vs. V*. We can now evaluate $\Delta\Phi_o$ from the experimental data of Figure 11 and Equation (9). The result is presented in Figure 12. The intercept of the linear regression with the ordinate gives the extrapolated value of $\Delta\Phi_o$, which turns out to be 1.70, well in agreement with the predicted value, $\Delta\Phi_o = 1.81$.

This is sufficient to evaluate the electrically controlled birefringence, taking into account Figure 12 and Equations (5), (6) and (9): $\Delta n_{\text{eff}}(E)$ is plotted in Figure 13 as a function of the square applied electric field.

From Figures 12 and 13 we can conclude that the electrically controlled birefringence at $E << E_c$, where E_c is the critical field for helix unwinding at zero frequency[1], is with a high level of confidence (99%) proportional to the square field E^2, as we experimentally demonstrated for the first time [20].

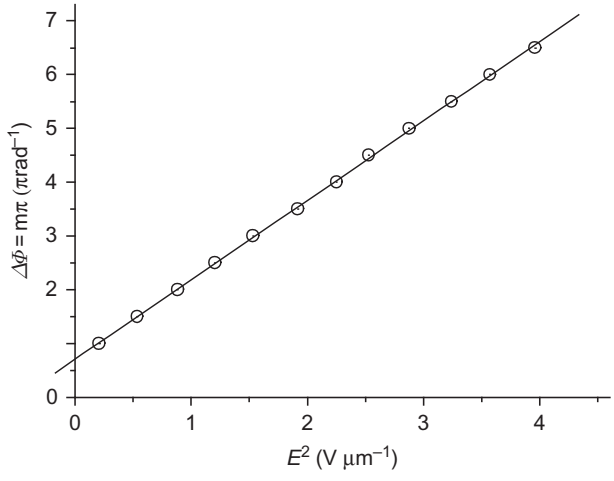

Figure 12. Phase shift $\Delta\Phi(E)$ dependent on the square applied field evaluated from data shown in Figure 11 and Equation (9).

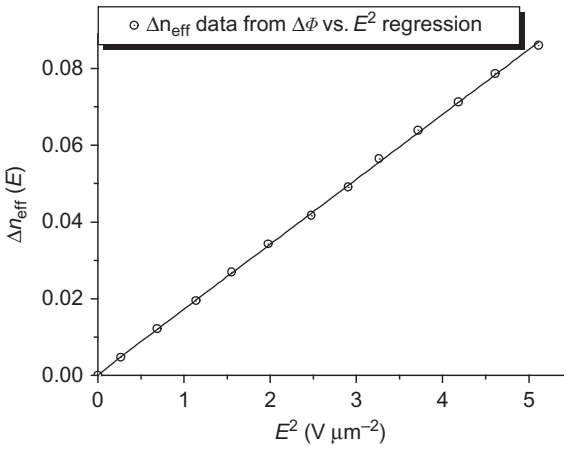

Figure 13. Dependence on the square applied electric field of the electrically controlled birefringence of a 44 μm cell filled with FLC-579.

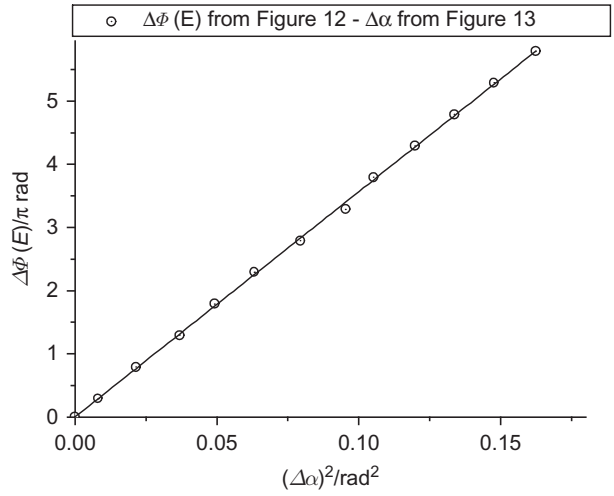

Figure 14. Dependence on the helix axis square rotation of the electrically controlled phase shift of the polarised light beam ($\lambda = 0.65$ μm) passing through 44 μm-thick DHF cell filled with FLC-579.

It is possible also to use this result to evaluate the material parameter G, and hence the critical field E_c, the susceptibility of Goldstone mode and the elastic constant K. In fact, we have shown (see Appendix, Equation (13A)) that the expected trend of the electrically controlled birefringence, in the hypothesis of $E << E_c$ and θ definitely smaller than 45°, is increasing with the square applied electric field, the angular coefficient B of the linear regression $\Delta n_{\mathrm{eff}(E)}$ vs. E^2 being dependent on the birefringence Δn, on the smectic polar angle θ, and on the material parameter G.

The angular coefficient of the linear regression reported in Figure 13 allows us to obtain an indirect measure of G, following a different experimental method with respect to that leading to the results shown in Table 2. As a consequence, the critical field E_c at zero frequency, the susceptibility χ_G of Goldstone mode, and the elastic constant K can also be evaluated in such a manner. From the regression data of Figure 13 we have $B = 0.017$ (μm V^{-1})^2. The birefringence of the unwound helix for FLC-579 is $\Delta n = 0.20$, since $n_{\|} = 1.70$, $n_{\perp} = 1.50$. The parameters evaluated are reported in Table 4, which is in good agreement with the results of Table 2. The susceptibility values are consistent with the results obtained with direct measurements performed in our laboratory, which will be published in another paper.

Table 4. Indirect measurement of the material parameters from experimental data relevant to electrically controlled birefringence.

DHF-cell thickness (μm)	G (μm/V)	E_c (V/μm)	χ_G	K (10^{-11}N)
44	0.2562	1.2	35	2.4

It is interesting to underline the theoretical result (see Appendix, Equation (24A)) illustrated by experimental data in Figure 14: the applied electric field drives the phase shift (and consequently the birefringence) only through the rotation of the anharmonic helix axis.

The angular coefficient B^* of the linear regression in Figure 14, modelled in Equation (25A), which provides the electrically controlled birefringence *vs.* the square rotation of the helix axis is given by

$$B^* = 4\Delta n\left(1 - \frac{3}{2}\sin^2\theta\right). \tag{11}$$

The expected value of the angular coefficient is $B^* = 0.48$, whereas its experimental value can be estimated as $B^* = 0.6 \pm 0.2$, being very dependent on the experimental uncertainties on $\Delta\alpha^2$ for very small values of E.

4. Discussion

Optical measurements of polarised light transmission through DHF cells 16 μm and 44 μm thick filled with FLC5-79 have been carried out, driving the cell via a voltage step function with various magnitudes at 1 kHz. There was found first of all that the application of a step function induces an anharmonic deformation providing the rotation of the helix axis towards one sense, due to the positive peak; and symmetrically towards the other sense, due to the negative peak. As the first main result, we confirmed experimentally that the rotation is rather small (< 20° per 60 V applied to the 16 μm cell) and linear with the field amplitude, as

predicted by Abdulhalim *et al*. [11], implementing this theory to the case when the polar angle θ, being smaller than 45°, is neither negligible nor close to 45° (for the FLC material under investigation $\theta = 31°$).

Moreover, we confirmed within 2% of average accuracy the validity of Malus' law in all measurements, allowing us to claim that the sample biaxiality is negligible, and to define ellipticity simply as $e \equiv \sqrt{I_{\min}/I_{\max}}$, in the cases e_+, (e_), i.e. when the positive (negative) voltage peak is considered. We then measured the ellipticity of both cells at the angle $\alpha_+ = 0°$ ($\alpha_+ = 90°$) between the actual helix axis and the polariser, in order to establish the optical quality of the cells, obtaining only $e = 0.17$ for the 16 μm cell and $e = 0.07 \div 0.10$ for the 44 μm cell, which turned out to be very well aligned.

At this point, the second main result was achieved by investigating the ellipticity of both cells when a step voltage at increasing intensity was applied, by putting the electric field of the impinging light beam at 45° with respect to the main optical axis of the DHF cell:

1. The thinner cell ellipticity oscillated between $e_{\min} = 0.17$, $e_{MAX} = 0.89$, whereas the ellipticity of the thicker cell, with better initial alignment, oscillated regularly between $e_{\min} = 0.10$, $e_{MAX} = 1.00$ due to the application of the step voltage with increasing amplitude, from 0 to 200 V_{pp}. Hence, the 44 μm cell birefringence was demonstrated to be modulated accordingly, behaving as a λ-optical layer when reaching the first minimum of ellipticity, then moving to the first maximum as $3\lambda/4$, then to the second minimum as $3\lambda/2$, etc;
2. The ellipticity measurements allowed us to evaluate the retardation $\Delta\Phi(E)$ *vs*. the applied voltage V and, consequently, the effective electrically controlled birefringence $\Delta n_{\text{eff}}(E)$;
3. Starting from the theory of Abdulhalim *et al.* [11], we predicted such a parameter to be proportional to the square applied electric field. Our experimental investigation completely confirmed our prediction: the electrically controlled modulation behaves as a Kerr effect as well $\Delta n_{eff}(E) \propto E^2$. By extrapolation to $E \to 0$ the retardation $\Delta\Phi_o$ at $E = 0$ has been evaluated and the undisturbed helix effective birefringence $\Delta n_{\text{eff}}(E = 0)$ has been obtained. Combining the two main results, we recognised that the electric field modulates the controlled birefringence$\Delta n_{\text{eff}}(E)$ only through the rotation of the anharmonic helix axis, turning out to be a composed linear function of E^2 only via $\tan^2 2\Delta\alpha$. Furthermore, the linear dependency of $\tan 2\Delta\alpha$ on E and the proportionality $\Delta n_{\text{eff}}(E) \propto E^2$ provide two independent methods for obtaining an indirect experimental measure of the material parameter $G \equiv \frac{\varepsilon_o \chi_G}{P_S}$, and two sources for evaluating the critical field at zero frequency E_c, the Goldstone susceptibility χ_G, and the elastic constant K.

Eventually, the polarised light transmission measurements permit the evaluation of the electrically controlled birefringence via ellipticity: we established a definite protocol concerning this type of investigation, illustrating the optical quality, the electro-optic behaviour of a DHF electrically modulated birefringent layer, defining the material parameter *G,* useful for describing the Goldstone mode, and suggesting two independent methods for measuring it.

5. Conclusions

Good alignment quality of cells filled by short helix pitch (330 nm) FLC was obtained with layer thicknesses of 16 μm and 44 μm. The alignment quality was characterised by a contrast ratio of 300:1, because of complete suppression of scattering and selective reflection of light in the visible spectral range, as the helix pitch was smaller than the wavelengths of visible light. In this work, FLC layers of this type have been shown to behave as quality electrically controlled phase retarders of visible light, and their electro-optical properties have been investigated.

–It was experimentally shown that the FLC layer biaxiality is negligible, allowing us to use the simplest method of measuring the ellipticity of light passing through the layer.
–For the first time, the electrically controlled phase retardation $\Delta\Phi(E)$ of the light transmitted and the effective birefringence $\Delta n_{\text{eff}}(E)$ of the DHF layer helical structure have been evaluated via ellipticity measurements.
–It was experimentally and theoretically shown that both $\Delta\Phi(E)$ and $\Delta n_{\text{eff}}(E)$ are proportional to the square applied electric field: $\Delta\Phi(E) \propto E^2$, $\Delta n_{\text{eff}}(E) \propto E^2$.
–For the first time the linear dependency on the field of the angular displacement of the helical axis $\Delta\alpha(E) \propto E$ in DHF effect was experimentally proven and theoretically confirmed.
–New experimental methods for evaluation of the helix dielectric susceptibility χ_G and elastic modulus K relevant to the Goldstone mode have been grounded on the basis of theoretical $\Delta n_{\text{eff}}(E)$ and $\Delta\alpha(E)$ dependencies, and of the data fitting according to the relevant models.
–The key role of the parameter $G \equiv \frac{\varepsilon_o \chi_G}{P_S}$ in electro-optics of DHF effect has been proved.

We plan to apply this method (i.e. measuring the intensity and the ellipticity of the transmitted light *vs.* the amplitude of the applied electric field) to obtain the rotation of the anharmonic helix axis and the electrically controlled birefringence in a number of DHF cells with different thicknesses, in order to investigate the role played in such phenomena by the anchoring energy.

Appendix

Theoretical evaluation of electrically controlled birefringence and helix axis rotation *vs.* electric field

To write the total phase shift in Equation (6) as the sum of the phase shift in the absence of an applied electric field plus the variation of the phase shift due only to the application of it, is always valid. However, it is interesting to introduce an approximation, which is allowed only if the smectic polar angle θ is smaller than 45°, the actual electric field E provided via the step function is smaller than the critical electric field for helix unwinding at zero frequency E_c, and the angular frequency ω of the step function is smaller than a characteristic angular frequency ω_m of the FLC material. In this approximation, according to Abdulhalim and Moddel [11], the average total birefringence reads

$$\Delta n_{\text{eff}} \equiv \langle n_e(\theta, \varphi_c(E;x)\rangle - n_o = \Delta n\left[1 - \frac{3}{2}\sin^2\theta + \frac{\sin^2 2\theta}{1-\frac{3}{2}\sin^2\theta} J_{-1}^2(a)\right], \quad (1A)$$

where $\Delta n \equiv n_e - n_o$ is the difference between the extraordinary and the ordinary index of refraction, $J_{-1}(a)$ is the Bessel function of the first kind of a small t-argument $a(t)$ involving the applied field E, its angular frequency ω and both E_c, ω_m:

$$a(t) = \frac{a_0}{1+\left(\frac{\omega}{\omega_m}\right)^2}\left(\cos\omega t + \frac{\omega}{\omega_m}\sin\omega t - \exp(-\omega_m t)\right), \quad (2A)$$

with

$$a_o = (\pi^2/16)(E/E_c). \quad (3A)$$

In Equations (2A) and (3A) the critical field E_c and the characteristic angular frequency ω_m, written in International System (SI), are given by

$$\begin{cases} E_c = \frac{\pi^2}{16}\frac{kq_o^2}{P_S} \\ \omega_m = kq_o^2/\gamma_\varphi \end{cases}, \quad (4A)$$

where

$$k \equiv \sin^2\theta(K_T\sin^2\theta + K_B\cos^2\theta) \quad (5A)$$

is an elastic parameter given in terms of a mean elastic constant between twist and bend K_T, K_B, $q_o \equiv 2\pi/p_o$ is the helix wave vector and γ_ϕ the rotational viscosity.

In one elastic constant approximation, $K_T = K_B \equiv K$, and Equation (5A) reads

$$k = K\sin^2\theta, \quad (6A)$$

and system (4A) becomes

$$\begin{cases} E_c = \frac{\pi^2}{16}\frac{K\sin^2\theta q_o^2}{P_S} \\ \omega_m = K\sin^2\theta q_o^2/\gamma_\varphi \end{cases}. \quad (7A)$$

In the static limit, which is roughly satisfied, since we operate at 1 kHz and the characteristic frequency is expected to be about 2.3 kHz, being $K \sim 3 \times 10^{-11}$ N, $\theta = 31°$, $p_o = 0.33$ μm, $\gamma_\phi = 0.2$ Pa s, $P_S = 120$ nC cm^{-2}, as we have previously measured all these parameters, one can suppose

$$\frac{\omega}{\omega_m} \to 0,\ \omega_m t \to \infty,\ \omega t \to 0. \quad (8A)$$

Hence from Equation (2A) the argument $a(t) \approx a_o$ and Bessel function can be reduced to its first term,

$$J_{-1}(a_o) = -\frac{\pi^2}{32}\cdot\frac{E}{E_C}, \quad (9A)$$

provided the hypothesis $E < E_c$ is satisfied. This means that it is necessary to estimate E_c in the frame of the approximated theory, not considering the data which do not satisfy the previous hypothesis for evaluation of any parameter. By expressing the Bessel term (9A) as a function of the helix dielectric susceptibility χ_G relevant to the Goldstone mode, following Urbanc *et al.* [21]:

$$\chi_G = \frac{P_S^2}{2\varepsilon_o K\sin^2\theta q_0^2}, \quad (10A)$$

where ε_o is the vacuum permittivity, we get

$$J_{-1}(a) = -\left(\varepsilon_o\frac{\chi_G}{P_S}\right)E. \quad (11A)$$

Eventually the effective birefringence is obtained as

$$\Delta n_{\text{eff}} = \Delta n\left[1 - \frac{3}{2}\sin^2\theta + \frac{\sin^2 2\theta}{1-\frac{3}{2}\sin^2\theta}\left(\frac{\varepsilon_o\chi_G}{P_S}\right)^2 E^2\right], \quad (12A)$$

and the contribution to the effective birefringence due only to the application of E is

$$\Delta n_{eff}(E) = \Delta n \frac{\sin^2 2\theta}{1 - \frac{3}{2}\sin^2\theta} G^2 E^2. \tag{13A}$$

Thus, the effective birefringence is predicted to increase, in the frame of the present approximation, as proportional to the square applied electric field, as was found experimentally by us. The angular coefficient B of the linear regression giving $\Delta n_{\text{eff}}(E)$ *vs.* E^2 computed by the experimental data where $E < E_c$, i.e.

$$B = \Delta n \frac{\sin^2 2\theta}{1 - \frac{3}{2}\sin^2\theta} G^2 \tag{14A}$$

depends on the birefringence Δn, on the smectic polar angle θ, and on the material parameter:

$$G \equiv \frac{\varepsilon_o \chi_G}{P_S}. \tag{15A}$$

This allows us to obtain from measurements of ellipticity used to describe the electrically controlled birefringence an indirect measurement of G and then of χ_G, knowing θ and P_S. Moreover, Equations (10A) and (15A) show that we can also obtain in the same way an indirect measurement of the elastic constant K:

$$G = \frac{P_S}{2K \sin^2\theta q_o^2}. \tag{16A}$$

In any case, combining Equations (9A) and (11A) with definition (15A) we get

$$G \equiv \frac{\pi^2}{32 E_c}, \tag{17A}$$

demonstrating that E_c can be also evaluated through electrically controlled birefringence.

Unfortunately, according to Equation (14A) it is not possible to plane a FLC mixture with an angle θ chosen for maximising the electrically controlled birefringence $\Delta n_{\text{eff}}(E)$, since the angular coefficient B for a fixed value of parameter G does not exhibit a relative maximum in the range from 0° to 45°, being simply an increasing function of θ. In the frame of the same approximation [11] the anharmonic helix axis rotation reads

$$\tan 2\Delta\alpha = \frac{\sin 2\theta \frac{\pi^2 E}{32 E_c}}{1 - \frac{3}{2}\sin^2\theta \left(1 - \frac{\pi^4 E^2}{1536 E_c^2}\right)}. \tag{18A}$$

Equation (18A) can be further simplified to

$$\tan 2\Delta\alpha = \frac{\sin 2\theta G E}{1 - \frac{3}{2}\sin^2\theta}, \tag{19A}$$

meaning that, in the hypothesis $E < E_c$, $\tan 2\Delta\alpha$ is proportional to the applied electric field, which, as a further approximation, implies that for very small values of the field the curve $\Delta\alpha$ *vs.* E can be considered as a straight line too, with angular coefficient b given by

$$b = \frac{\frac{1}{2}\sin 2\theta G}{1 - \frac{3}{2}\sin^2\theta}. \tag{20A}$$

From Equation (20A) we could also derive a direct dependency of b on the critical field E_c,

$$b = \frac{\frac{\pi^2}{64 E_c}\sin 2\theta}{1 - \frac{3}{2}\sin^2\theta}, \tag{21A}$$

on the susceptibility χ_G,

$$b = \frac{\varepsilon_o \chi_G \sin 2\theta}{P_S\left(1 - \frac{3}{2}\sin^2\theta\right)} \tag{22A}$$

and on the elastic constant K,

$$b = \frac{\frac{1}{2} P_s \cot\theta}{K\left(1 - \frac{3}{2}\sin^2\theta\right) q_o^2}. \tag{23A}$$

Notice that Equation (19A) is expressed in terms of the same material parameter $G \equiv \frac{\varepsilon_o \chi_G}{P_S}$ introduced in Equation (13A) concerning the electrically controlled birefringence, having taken into account the critical field (7A), and the susceptibility (10A). The relationship (19A) shows that only one parameter G, which is related to FLC material and to allowance for azimuthal rotation, describes both the helix axis deviation due to the applied electric field and the electrically controlled birefringence. This means that the second phenomenon is simply a consequence of the first, as is demonstrated, substituting Equation (19A) into Equation (13A), by the fact that E provides birefringence modulation only through $\Delta\alpha$,

$$\Delta n_{\text{eff}}(E) = \Delta n \left(1 - \frac{3}{2}\sin^2\theta\right) \tan^2 2\Delta\alpha, \tag{24A}$$

which can be simplified to

$$\Delta n_{\text{eff}}(E) = 4\Delta n \left(1 - \frac{3}{2}\sin^2\theta\right) \Delta\alpha^2(E). \tag{25A}$$

Furthermore, it should be emphasised that it is possible to use the two independent measurements of helix axis rotation *vs.* E and of electrically controlled birefringence *vs.* E for evaluating the same fundamental parameter G, obtaining from two sources indirect measurements of critical field at zero frequency E_c, of Goldstone susceptibility χ_G, and of elastic constant K.

Care should be paid in computing the linear regression angular coefficients B, b defined in (14A) and (20A), taking into account only experimental values satisfying the condition $E < E_c$.

Acknowledgements

The authors are very grateful to Ibrahim Abdulhalim, Ben-Gurion University of the Negev - Faculty of Engineering Sciences, for very useful suggestions. The work was supported by the Russian Foundation of Basic Research, grants NN 08-03-90009, 08-02-01074-a and grants: 07-07-91582-ASP_a, 08-03-90009-Bel_a, 07-02-96610-p; it was partially funded by Fondazione Cassa di Risparmio di Torino (FCRT) in the frame of the bilateral project Piemonte-Russia "Nanotecnologie per le industrie elettromeccaniche, dell'informazione e del medicale (FCRTnano)". One of the authors (C.A.R. Yednak) acknowledges a grant from Coordenadoria de Aperfeiçoamento de Pessoal de Nível Superior (CAPES), Paranà, Brasil; another author (S. Torgova) acknowledges Politecnico di Torino, Dipartimento di Fisica, for financial support.

References

[1] Kuczynski, W.; Stegemeyer, H. *Chem. Phys. Lett*. **1980**, *70*, 123–126.

[2] Beresnev, L.A.; Blinov, L.M.; Baikalov, V.A.; Pozhidaev, E.P.; Pavluchenko, A.I.; Purvanetskas, G.V. *Mol. Cryst. Liq. Cryst*. **1982**, *89*, 327–338.

[3] Loseva, M.; Chernova, N.; Rabinovich, A.; Pozhidaev, E.; Narkevich, J.; Petrashevich, O.; Kazachkov, E.; Korotkova, N. *Ferroelectrics* **1991**, *114*, 357–377.

[4] Chernova, N.I.; Loseva, M.V.; Pozhidaev, E.P.; Korotkova, N.I. *Ferroelectrics* **1993**, *138*, 95–101.

[5] Haase, W.; Ganzke, D.; Pozhidaev, E.P.; Ozaki, M.; Matsui, T.; Nakajama, K.; Joshino, K.J. *Soc. Mat. Eng*. **2000**, *9*, 95–96.

[6] Pozhidaev, E.P.; Torgova, S.I.; Molkin, V.M.; Minchenko, M.V.; Vashchenko, V.V.; Krivoshey, A.I.; Strigazzi. A. *Mol. Cryst. Liq. Cryst.* **2009**, *509*, 1042–1050.

[7] Beresnev, L.A.; Chigrinov, V.G.; Dergachev, D.I.; Pozhidaev, E.P.; Fünfschilling, J.; Schadt, M. *Liq. Cryst.* **1989**, *5*, 1171–1177.

[8] Haase, W.; Ganzke, D.; Pozhidaev, E.P. *Mat. Res. Soc. Symp. Proc*. **1999**, *599*, 15–26.

[9] Panarin, Yu.P.; Pozhidaev, E.P.; Chigrinov, V.G. *Ferroelectrics* **1991**, *114*, 181–186.

[10] Pikin, S.A.; Indenboom, V.L. *Ferroelectrics* **1978**, *20*, 151–156.

[11] Abdulhalim, I.; Moddel, G. *Mol. Cryst. Liq.Cryst.* **1991**, *200*, 79–101.

[12] Panarin, Yu.P.; Pozhidaev, E.P.; Barnik, M.I. *Mol. Mat.* **1992**, *1*, 29–42.

[13] Hecht, E. *Optics*; Addison Wesley: Reading, MA, USA, 2002.

[14] Rossi, B. *Optics*; Addison Wesley: Reading, MA, USA, 1957.

[15] Clark, N.A.; Lagerwall, S.T. *Appl. Phys. Lett*. **1980**, *36*, 899.

[16] Pozhidaev, E.P.; Pikin, S.A.; Ganzke, D.; Shevtchenko, S.A.; Haase, W. *Ferroelectrics* **2000**, *246*, 235–245.

[17] Pozhidaev, E.; Chigrinov, V.; Du, T.; Kotova, S.; Minchenko, M.; Vashchenko, V.; Krivosey, A.; Fei, F. *Proceedings of the 28th International Display Research Conference*, Rome, Italy, September 2009; p 41.

[18] Fünfschilling, J.; Stalder, M.; Schadt, M. *SID-99 Digest* **1999**, 308–311.

[19] Fünfschilling, J.; Stalder, M.; Schadt, M. *Ferroelectrics* **2000**, *244*, 257–264.

[20] Pozhidaev, E.P.; Strigazzi, A.; Torgova, S.I.; Minchenko, M.V.; Miraldi, E. *Proceedings of the 10th European Conference on Liquid Crystals*, Colmar, France, April 19–24, 2009; p 175.

[21] Urbanc, B.; Zheksh, B.; Carlsson, T. *Ferroelectrics* **1991**, *113*, 219–230.